Washable Oil-Coated Structured Support For Passive Outdoor Particulate Matters Trapping

Tuan-Hoang Trinh,[a] Charlotte Pham,[b]* Jean-Mario Nhut,[a] Fabrice Vigneron,[a] Christophe Vieville,[c] Nicolas Reiminger,[d,e]* Xavier Jurado,[d] Housseinou Ba,[a] Thierry Romero,[a] Lai Truong-Phuoc,[a] Nicolas Hertel,[f] Christophe Legorgeu,[d] Loïc Vidal,[g] Cuong Pham-Huu[a,]*

(a) Institute of Chemistry and Processes for Energy, Environment and Health (ICPEES), UMR 7515 of the CNRS-University of Strasbourg, 25 rue Becquerel, 67087 Strasbourg cedex 02, France
(b) SICAT SAS, 20 place des Halles, 67000 Strasbourg, France
(c) ACM GmbH, Industriestrasse 1, B310, 77731 Willstätt, Germany
(d) AIR&D, 32 rue Wimpheling, 67000 Strasbourg, France
(e)ICUBE Laboratory, UMR 7357, CNRS/University of Strasbourg, 67000, Strasbourg, France
(f) TrapAparT SAS, 20 place des Halles, 67000 Strasbourg, France
(g)Institut de Science des Matériaux de Mulhouse (IS2M), UMR 7361 of the CNRS-Université de Haute-Alsace, 15, rue Jean Starcky, BP 2488, 68057 Mulhouse cedex, France

**Corresponding authors:*
nreiminger@air-d.fr (N. Reiminger)
charlotte.pham@sicatcatalyst.com (C. Pham)
cuong.pham-huu@unistra.fr (C. Pham-Huu)

Citation : Trinh, T.-H., Pham, C., Nhut, J.-M., Vigneron, F., Vieville, C., Reiminger, N., Jurado, X., Ba, H., Romero, T., Truong-Phuoc, L., Hertel, N., Legorgeu, C., Vidal, L., & Pham-Huu, C. (2024). Washable oil-coated structured support for passive outdoor particulate matters trapping. Sustainable Cities and Society, 116, 105884. https://doi.org/10.1016/j.scs.2024.105884

Abstract: Direct outdoor air depollution represents an interesting path for preventing indirect disease. In the present work, a simple and efficient PMs trapping media based on the use of an oil-coated structured polymer media was developed for passive trapping of various PMs, ranging from coarse (PM_{10}), to fine ($PM_{2.5}$) and ultra-fine (PM_1) dimension in outdoor environment. The device can be easily regenerated by a simple washing with a mixture of water and detergent followed by a new oil coating cycle. The total PM loading mass of the passive trap and the recovered PMs are analyzed through different techniques and confirm the great efficiency of such filter to trap various PMs when exposed to a high traffic road. The spent filter can be regenerated through a simple washing step and can be repeatedly re-used with similar PM loading mass. The high and long-lasting total PM loading mass were also supported by numerical simulations based on computational fluid dynamics, also used to propose an optimization implementation of such system for future deployment at scale.

Keywords: particulate matter, passive, filter, trapping, air quality

Highlights

- Passive outdoor filter with high efficiency for trapping fine and ultrafine PM
- Regenerable filter for outdoor air depollution with easy implementation
- Combination of simulations and experimental data for large-scale deployment

INTRODUCTION

Particulate matter (PM) pollution, which is originated from concentrations of solids, liquids-solids or gas-solids/liquids emitted in the air by natural diasters or by anthropogenic activities, represent a major concern for human health [1–8]. PM is categorized by three main categories based on the diameter of particles, i.e., PM_1 (ultrafine), $PM_{2.5}$ (fine) and PM_{10} (coarse), which refer to particle sizes below 1, 2.5 and 10 μm, respectively. PM_1 and $PM_{2.5}$ pollution is particularly harmful since it can penetrate human bronchi and lungs owing to the small particle size [9,10]. Nowadays, the number of premature deaths attributed directly or indirectly to air pollution each year is around 8 million for both outdoor and indoor air pollution according to the World Health Organization (WHO) [11]. In addition, the risks over human health are increased for people living in the vicinity of high-traffic roads where small and ultrafine particles, i.e. $PM_{2.5}$ and PM_1, are frequently observed and which can be carried by wind or turbulence from the vehicles far from the emission area [12–14]. Due to their harmful effects, PMs reduction in cities has received a high public interest in order to reduce as much as possible disease for the citizen [15,16]. Furthermore, reports also pointed out that about 30 % of the pollution by microplastic particles in rivers, lakes and oceans is originated from tire wear debris and will significantly increase in a proportional way to the number of Light Duty Vehicle (LDV) [17–19].

During the last decades, a large number of reports dealing with the PMs removal from outdoor air have been published [20–26]. However, most of them were based on the use of active filters which operated with an external energy input [27]. Active filtration is carried out using a fan or air extractor to force the airflow through the filter where the PM are trapped when it comes into contact with the filter device. In addition to such mechanical capture some proactive capture processes are also developed to improve the trapping efficiency by charging the PM with an ioniser or by using advanced filtration materials with high dipole moment to improve the capture through chemical forces. Such filtration mode is frequently used for indoor as well as for outdoor depollution [28–33]. However, active filters present several drawbacks: (i) the system must be connected to an external energy source to powering the air flow through the filter, or, to induce charging of either the PM or the filter; The primary issue is that in certain specific locations, such as open urban areas or underground train stations where electrical connections are tightly regulated, it is not always possible to access an external energy source to power the system, (ii) the air extractor generates a relatively high noise which could pose problem for the neighbouring, especially at night, and (iii) active filtration devices usually uses small aperture filters which can be rapidly plugged with low amount of PMs trapped inducing large pressure drop across the filter and necessitate short-term replacement. It is anticipated that replacing active filtration devices with passive ones for PM reduction will be of great interest, as they are less energy-intensive and more environmentally friendly. On the other hand, passive filter are relatively inexpensive, require no electricity to operate, and can be deployed at numerous locations easily and cost-effectively. The possibility of regenerating the spent filter and reuse also represent interesting environmental and economic alternatives with respect to active filtration devices. Some passive filters have been developed based on the use of weblike electrospinning structure which displays a high total PM loading mass [34–36]. The main drawbacks of the electrospinning filters are the relatively high-pressure drop and that they cannot be effectively regenerated, thus hindering their industrial development for large-scale deployment. On the pathway for understanding and finding solutions for PM mitigation in urban environments, experimental and computational studies are needed. The danger of PMs and associated methods for PMs characterization in urban environments were highlighted [37–40]. Solutions of outdoor PM filtration were tested such as active PM tower filtration [15,28], vegetation PM filtration [38], etc. Computational fluid dynamics (CFD) models are becoming a useful method to simulate air pollution. Reiminger and Jurado et al. [41–

43] computed models of air pollution, while using deep learning methods to compute spatial data, a promising pathway in air pollution study.

In the present work, a PMs trapping media has been put under experiments for passive trapping of PMs in the outdoor environment, which can be reused after a washing step to remove the trapped PMs [44,45]. The system is simple for operating and consists of a structured polymer media coated with vegetable oil which traps the PM when it encounters the surface. The trapping experiments were carried out directly in an open space located next to a high traffic road crossing the city of Strasbourg, France, with high frequency of stop-and-go significantly consuming brakes and tires. The device can be regenerated by a simple washing with a mixture of water and detergent followed by a new coating cycle. The total PM loading mass of the passive trap as a function of exposure duration, and the recovered PMs are analysed through different techniques as well as numerical simulations regarding the future deployment of such systems at a bigger scale. The main purpose of this paper is double: verifying the oil coating concept of air filtration, and testing the passive PM capture on the near-source outdoor environment. As described in [46,47], the oil coating layer is used for enhancing PM capture and retention on a low pressure drop filter structure. This work aim is not to develop a brand new air filter, but to demonstrate the real potential of this concept in PM capturing in various complicated environments like outdoor. Different from indoor air filtration, outdoor or semi-closed spaces like parkings are frequently subject to many weather parameters and PM variations, adding to limits of material choices and energy source installation. Based on weather conditions and nature of PM emissions, materials of filter structure and oil coating can be carefully selected in order to have the maximum performance without conflicting with the safety norms of the location. The materials and labour costs can vary depending on country and market situation, but the choice of a regenerable material may reduce environmental impacts while keeping its effectiveness.

■ METHODS

Materials. The passive PM trapping process was carried out using an open box which can host twenty filters and different sensors to monitor the different parameters implemented next to an urban area with high PM pollution (Fig. 1A and B). The schematic representation of the whole filtration device is displayed in Fig. 1C for the sake of clarity. The media is consisted with commercial polyester (hereafter noted “Aerosleep”) structured host matrices with large exposure surface area to offer a maximum surface contact between the polluted air and the trapping media (Fig. 1D) alongside with an extremely low-pressure drop. The PM total PM loading mass was significantly improved by depositing a thin layer of vegetable oil, on the topmost surface of the host substrate (Fig. 1E & 1F). The oil layer with sticky properties allows one to harvest any PMs which come in contact with the media regardless their size and shape as well as nature, i.e., organic, inorganic or even living matter such as pollen or insect with size ranged from tenths few nanometers to several hundred micrometers or even millimeters. The PMs trapping was realized through contact between the PM airborne and the filter surface and it is mostly depending on the outdoor air flow rate passing through the filter media.

Characterization Techniques. The samples, fresh and spent, were characterized by different techniques to investigate the characteristics of the media and the quantity, nature and size distribution of the trapped PMs.

Scanning electron microscopy (SEM). Analyses were carried out on a ZEISS 2600F microscope with a resolution of 5 nm. A sample with the following dimension was analyzed: width, 10 mm, length, 10 mm, thickness, 6 mm. Before analysis, the sample was oven dried at 60 °C for overnight in order to reduce the oil layer thickness which could hinder the detail analysis of the trapped PMs. The sample was deposited onto a

double face graphite tape to avoid charging effect during the analysis. For each sample, statistical analysis with different magnifications were carried out on at least four zones in order to provide a global distribution of the trapped PMs. The statistical SEM results were also used for the measurement of the PM size distribution and compared with that determined by DLS technique.

Pressure drop measurements. Experimental pressure drops (ΔP) across each sample was measured using a home-made apparatus consisting with a tubular reactor with the following dimension: 80 cm high, 4 cm internal diameter. The sample is located at the middle of the set-up and hold by a ring seal on both sides to maintain it steady during the different measurements. Gas velocity is measured with anemometer Testo 435-1 equipped with hot wire probe (0–20 m/s). Hot wire probe, due to its small diameter, was chosen to limit the gas flow perturbation. Pressure drop was measured with differential pressure sensors (Digital Manometer Ehdis CR410). Pressure drop was measured on 6 mm long foam varying the gas velocity in the 0–10 m/s range.

Viscosity characterisation protocol. The oil viscosity was measured with a TA Instrument DHR3 rheometer containing a Pelletier disc. For each sample, 0.6 ml of liquid was taken to perform two tests: viscosity as a function of temperature and as a function of shear rate. In the first test, the viscosities of the oils were measured at a fixed frequency (10 rpm for 20 minutes), with the temperature ranging from -15˚C to 80˚C. On the other hand, the temperature in the second test was fixed at 40˚C with the shear rate gradually increasing (frequency ranging from 3 to 50 rpm for 5 minutes). Before each test, the sample was conditioned for 2 minutes to ensure good homogeneity in temperature and density (absence of air bubbles that could influence the measurement). Between two consecutive analyses, the Pelletier disc was cleaned with ethanol and acetone.

Transmission electron microscopy (TEM). Analysis were carried out on a JEOL ARM-200F working at 200 kV accelerated voltage, equipped with a probe corrector for spherical aberrations, and a point-to-point resolution of 0.2 nm. The sample was dispersed by ultrasounds in an ethanol solution for 5 minutes and a drop of the solution was deposited on a copper covered with a holey carbon membrane for observation.

Dynamic Light Scattering (DLS). 5 mL of the suspension is sampled from the homogenised mixture of washing solution for DLS analysis. Analyses were carried out on a granulometer MALVERN Mastersizer 3000 with water as solvent without any additives. The suspension was ultrasonicated for 2 min before analysis. The analysis was realized with a stirring and pumping speed of 50 % and the particles in the size ranged from 0.01 to 2,000 μm were analyzed.

Filter washing. Spent filter was treated with solution of 5-10% detergent (Alcohol C9-C11 ethoxylated, KOH) mixing with distilled water at 80°C, followed by 15 min ultrasonication. The washing cycle can be reapeated until no particle remain visible on the filter. After the washing step, filter can be dried in the oven at 60°C overnight before re-use, preceed by a new oil layer coating step.

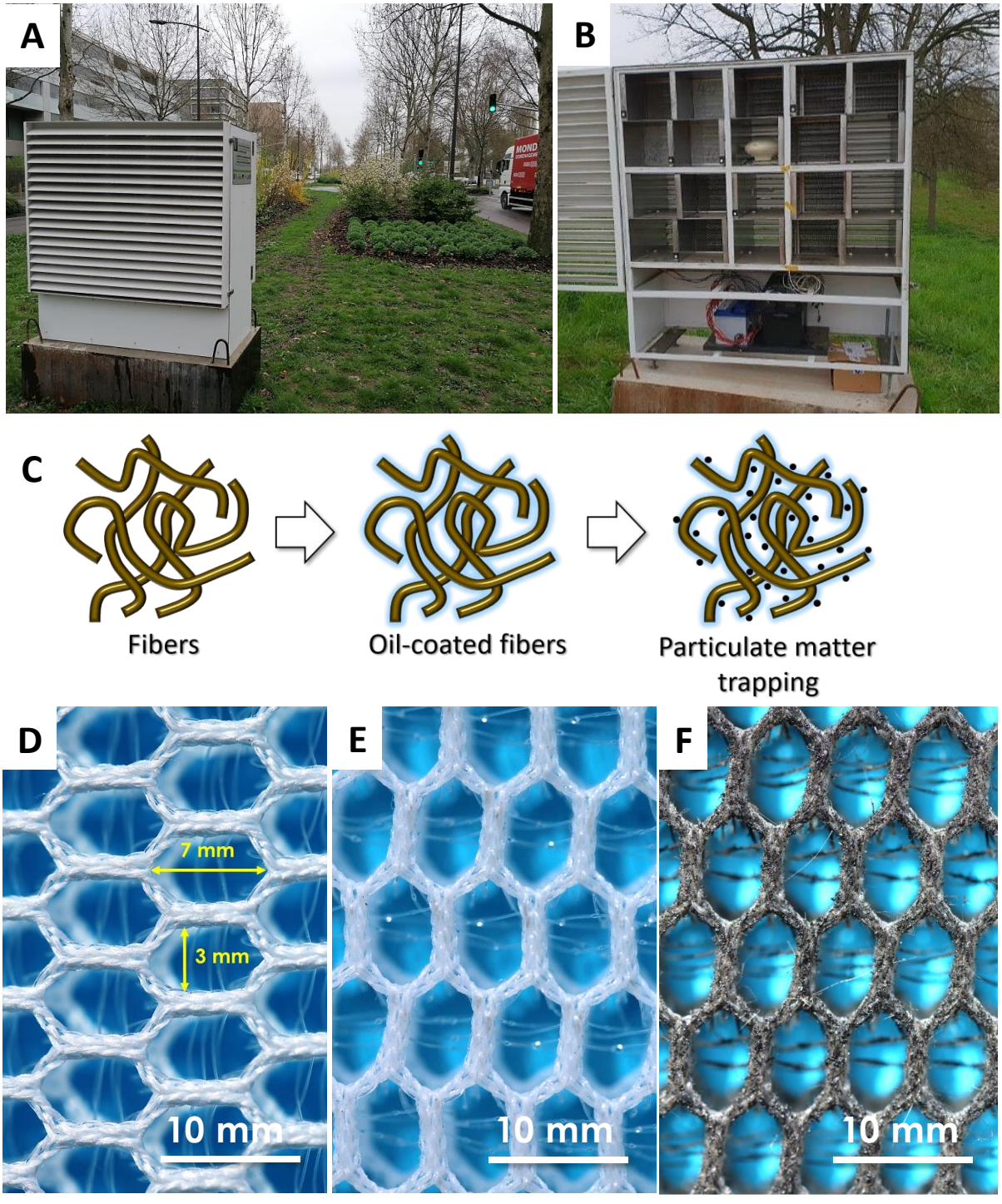

Fig. 1 | (**A**, **B**) Digital photos of the trapping device located in an urban area and the trapping media. (**C**) Schematic representation of the hosting device and the detailed structure of the passive filter. (**D**) Digital photo of the structured filter as received, (**E**) after coated with a thin and homogeneous layer of vegetable oil; some small oil beads can be observed on the intermediate plastic fibers within the large hexagonal aperture, and (**F**) after passive filtration for 4 weeks where the filter color has drastically changed from white to dark gray due to the presence of large number of PMs trapped on its surface.

Numerical simulations. Numerical simulations were carried out through Computational Fluid Dynamics (CFD) modeling using the Unsteady Reynolds-Averaged Navier-Stokes (URANS) methodology. The simulations were performed on OpenFOAM 9.0 with an unsteady solver validated for outdoor air quality assessment purposes in urban areas. This solver solves the continuity (E.1) and the momentum (E.2) equations from the Navier-Stokes' system as well as the advection-diffusion equation (E.3). These equations are given hereafter:

$$\nabla . u = 0 \qquad (1)$$

$$\frac{\partial u}{\partial t} + u . \nabla u = -\frac{1}{\rho}\nabla p + \nu \Delta u \qquad (2)$$

where u is the velocity [m.s^{-1}], p is the pressure [kg.m^{-1}.s^{-2}] and ν is the kinematic viscosity [m^2.s^{-1}] and t the time [s].

$$\frac{\partial C}{\partial t} + \nabla . (Cu) - \nabla . \left[\left(D_m + \frac{\nu_t}{Sc_t} \right) \nabla C \right] = E \qquad (3)$$

where C is the pollutant concentration [g.m^{-3}], u is the velocity [m.s^{-1}], D_m is the molecular diffusion coefficient [m^2.s^{-1}], ν_t is the turbulent viscosity [m^2.s^{-1}], Sc_t is the turbulent Schmidt number taken as 0.7, t is the time [s] and E is the emission of pollutants [g.s^{-1}].

To solve the Navier-Stokes equations using URANS methodology, the RNG k-ε turbulence closure scheme [48] has been used. The simulations were performed using second-order schemes, and the results were extracted after that the convergence was reached. All simulation results were obtained with residuals lower than 10^{-5}.
Finally, all the recommendations given by Franke et al. [49] for the simulation of flows in urban environments were followed, including:

- Lateral and vertical extension of the computational domain: the top of the computational domain is located at a minimum distance of 5 × H from the highest building and the lateral, inlet and outlet boundaries at a minimum distance of 5 × H from the closest building (with H the height of the highest building in the domain).
- Mesh independence: mesh of 0.5 m near the buildings and the ground were used as they ensure sufficient mesh-size independence for urban environment modeling [50].
- Boundary conditions: inlet velocity (E.4) and turbulence (E.5, E.6) profiles following Richard and Norris recommendations [51], symmetry conditions for the top and lateral boundaries and a free stream condition for the outlet.
-

$$U(z) = \frac{u_*}{\kappa_{k-\varepsilon}} ln\left(\frac{z + z_0}{z_0}\right) \qquad (4)$$

$$k(z) = \frac{{u_*}^2}{\sqrt{C_\mu}} \qquad (5)$$

$$\varepsilon(z) = \frac{{u_*}^3}{\kappa_{k-\varepsilon} . z} \qquad (6)$$

where U is the velocity [m.s^{-1}], k is the turbulent kinetic energy (TKE) [kg.m^{-1}.s^{-3}], ε is the turbulent dissipation rate [kg.m^{-1}.s^{-4}], u_* is the friction velocity [m.s^{-1}], z is the altitude [m], z_0 is the roughness length [m] taken to 0.5 m, C_μ is a CFD constant [-] taken to 0.09 and $\kappa_{k-\varepsilon}$ is the Von Kármán constant [-] taken to 0.41.

The approach and model described previously have been found to be able to reach errors which are less than 10% compared to experimental data as show in [52] were more details about the model validation can be found, and a similar approach has been proven to lead to an overall error of around 30% compared to a real situation in an urban area [53].

All the solid obstacles such as buildings present in the computational domain limits were 3D modeled. Two building layouts were considered, the first one without any trap (comparison case) and the second with a line of 50 traps (70 m long) placed between the modeled emission source (road lines) and an elementary school. Traffic emissions set up in the model were calculated using COPERT [54], a calculation method from the European Environment Agency (EEA) considering the French vehicle fleet, the traffic data available on the considered road (38.160 vehicles.day^{-1} including 8.5 % of heavy-duty trucks, and an averaged traveling speed of ca. 30 km.h^{-1}), and the road length in the model (290 m), which led to PM_{10} emission of around 23.22 g.h^{-1} under these assumptions.

PM_{10} trapping was simulated as a mass sink term considering a total PM_{10} reduction rate of 1.06 g.h^{-1} (experimental value) with a pressure loss inside the trap numerically modeled by the means of the Forchheimer law using F = 4.02 m^{-1} (experimental value).

Lastly, nine simulations were performed considering wind speed of 1.5 m.s^{-1} at 10 m high and coming from nine directions (from 20°N to 340°N with a 40° step), and the results were aggregated considering the continuous methodology described in [55,56] and the PM_{10} background concentration of Strasbourg (17 µg.m^{-3}) to obtain annual concentrations, allowing comparison with annual EU and WHO standards.

■ RESULTS AND DISCUSSION

Structured filter support and oil characteristics. The pressure drop measured on the Aerosleep structure under different air flow rate is benchmarked with those obtained on another filter for comparison (Fig. 2A). According to the results, the Aerosleep filter displays the lowest pressure drop even at relatively high linear velocity, i.e., 8 m.s^{-1}, among the evaluated materials such as random particles bed and open-cell foam [57]. For comparison, aluminum entangled filter was also evaluated, and the results are presented in the same figure. According to the results, the high-entangled aluminum structure displays a much higher pressure drop for a given linear space velocity (Fig. 2A). Such results reinforce the choice of Aerosleep as passive filters for the process as for such filter the total PM loading mass is directly dependent to the airflow passing through the filter and high-pressure drop would reduce the airflow leading to a low total PM loading mass. The oil-coated filter displays a very similar pressure drop behavior as a function of space velocity which indicates that pressure drop due to drag forces on the oiled surface is negligible (Fig. 2A). However, for passive trapping mode, the maximum airspeed remains relatively low, within the range of 2 to 4 m.s^{-1}, and thus, leads to a small pressure drop across the filter. It has been reported by Zhang et al. [25] that the total PM loading mass increases on a fibrous membrane with high entangled structure but with a detrimental increase of the pressure drop across the set-up.

The evaporation rate and the intrinsic viscosity are important parameters while investigating a liquid behavior deposited on a solid substrate. As evaporation is an endothermic process and based on kinetic energy of individual particle [58], weak connection molecules such as water or gasoline with short hydrocarbon chains can evaporate over time depending to the external parameters such as temperature, pressure and relative humidity, even when the external medium not reaching the boiling point [59]. Moreover, mineral or vegetable oil have higher boiling point and evaporate slower than water and gasoline in the same conditions [60]. Olive oil contains mostly long chains of fatty acids such as triglycerides, which require high energy to break-down the chain [61,62]. Olive oil can even be used for evaporation-retardant of the tear film lipid layer [63]. When the ambient temperature is far lower than the boiling point (180°C), evaporation of industrial stabilized olive oil used in this study, i.e. 35 mg. day^{-1} at 60 °C is considered insignificant in comparison to the gravitational dripping which is linked with the viscosity of the oil (Fig. 2B). The quantity of adsorbed oil on the trap sharply decreases within the first 2 days, due to the gravitational oil dripping, and remains almost unchanged after 10 days as shown in Fig. 2C which thus confirms that evaporation is not the main cause for the limited adsorption of PM after a prolonged exposure on-site (see results presented later on).

The adsorption capacity, expressed in terms of oil weight per surface area of the Aerosleep and the aluminum filter (for comparison) with smaller apertures, was also evaluated and the results are presented in Fig. 2C. The results clearly show higher oil retention in the Aerosleep structure, which could be attributed to some physical retention between the entangled polymer filaments, compared to that obtained on the aluminum structure where lower interaction is expected. Such results confirm the advantage of using a large pore Aerosleep filter for passive outdoor trapping.

Total PMs loading mass on passive filter. The PM specific total PM loading mass expressed per trapping surface ($g_{PM}.m^{-2}$) of the media filter measured as a function of time of exposure is presented in Fig. 3A. The PM trapped steadily increases with time of exposure and reaches ca. 55-60 $g.m^{-2}$ after about 16 weeks. It is worthy to note that some slight variation can be observed between the different traps which could be due to some inhomogeneity in the air passed through the filter located at different positions. The average PMs loading on the passive traps was calculated from the results obtained on several traps in order to assess the accuracy of the results. It is worthy to note that the error bars become wider with the trapping duration according to the results presented in Fig. 3A. Such results could be attributed to the change of the surface properties of the oil coated film as a function of the exposure duration due to the slowly dries-off of the oil surface. Indeed, at short-term adsorption the oil coated surface remains much sticky which displays higher and reproducible adsorption capacity for PMs, while at long-term adsorption the oil surface could be dried-off and thus, displays lower adsorption efficiency leading to a larger discrepancy between the different measures. However, the adsorption efficiency remains in good agreement with the time of exposure, at least up to 10 weeks, which confirms the advantage of the passive trapping device for outdoor PMs harvesting. The PMs loading attained about 60 g of $PM.m^{-2}$ which representing a relatively high loading value for passive adsorption. In addition, the large open structure associates with extremely low pressure drop of our filter also contribute to the avoidance of rapid filter plugging and cake filtration as usually encountered with traditional active filtration devices where low PMs loading could induce high pressure drop across the filter and necessitate higher pumping rate to compensate such phenomenon. Traditional HVAC electret media and nanofiber layer [64] or membrane filter [65] displayed rapid increase of pressure drop after a few gram of PMs loaded, which can lead to cake filtration or PM resuspension, or even the short-term replacement of the filter. The amount of PM slightly decreases afterward for the next consecutive test at 18 weeks. Such results could be explained by the fact that after 14 weeks, the oil layer becomes

dry which cannot provide any anchorage surface for trapping PM in the outdoor atmosphere while continuous exposing of the filter results in some PM loss due to the physical detachment of these later from the filter. It is worthy to note that such trapping tests were carried out for a relatively long duration (i.e., several weeks), which confirm the usability of such passive filter for real application. A digital photo of the Aerosleep filter after 18 weeks exposure is presented in Fig. 3B to highlight the dense deposit of PM and aggregates on its surface.

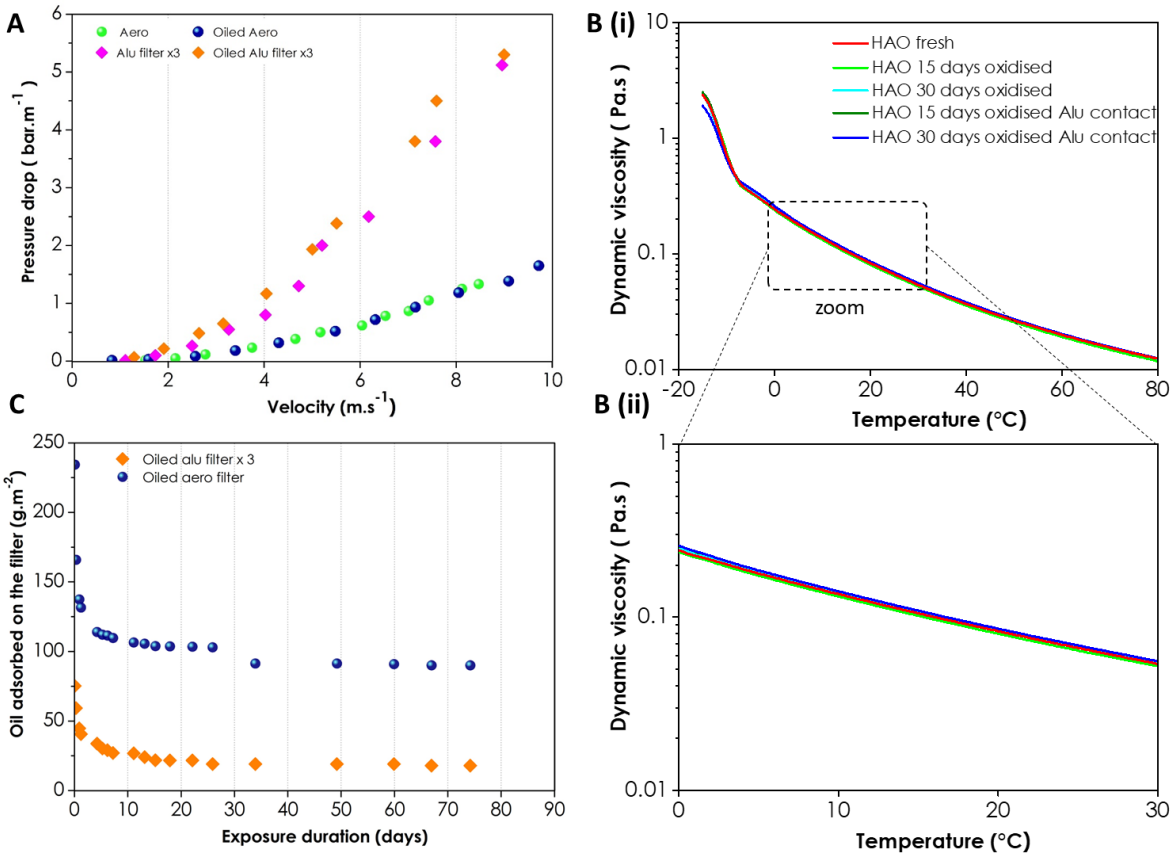

Fig. 2 | (A) Pressure drop measurements on the Aerosleep and an alternative aluminum structure, before and after the oil coating. The aluminum structure was used for highlighting the low-pressure drop across the Aerosleep filter which is the key factor for an efficient harvesting of the PM through such open filter. (B) i) Dynamic viscosity of the olive oil coated on Aerosleep filter vs. Aluminum filter as a function of the temperature. ii) Enlargement of the temperature region of exposure. (C) Oil adsorption capacity measured on the Aerosleep filter vs. an aluminum filter (g. m^{-2}) as a function of time.

Oil selection procedures were based on laboratory tests on different criteria of diverse vegetable and mineral oils. The preselection is inclined more toward vegetable oil for the reason of their origin, which is not harmful to human health through inhalation, in case of dispersion in air. Deodorized, stabilized industrial olive oil was taken as reference oil because of its weak odour, and stable viscosity after ageing while exposed to temperature and metal contact. The oil amount per filter surface experiment results is shown in Fig. 2C. Oil quantity decreases drastically after infiltration on filters due to gravity and slows down and forms a thin layer on filter structure, reaching approximately 150 ± 30 $g.m^{-2}$ on average. After 30 days of exposure, oil can slowly continue dripping, until reaches the stable oil level of 90 $g.m^{-2}$.

Other tested alternatives of olive oil such as sunflower oil (also deodorised and stable in viscosity but higher costs than olive oil) or aqua-soluble mineral oil (easier for washing and regenerable but stronger in odour and higher costs than olive oil) that can be taken into consideration for other outdoor or semi-closed spaces experiments. In Fig. 3H, during the same exposure duration, the coated filter yields much higher than the raw material as a filter support without the oil layer.

DLS analysis of the suspension recovered after water washing of a filter exposed for 8 weeks indicates that while fine and ultrafine particles represent a small proportion in the PM distribution by particles volume (Fig. 3C) they are accounting for a much higher proportion when expressed in distribution by numbers of particles (Fig. 3D). These fine and ultrafine particles are the most toxic ones as they easily enter in the alveoli in which clearance is much slower [66]. A similar trend is also observed for the samples with different exposure duration where fine and ultrafine PMs are clearly visible. The presence of fine and ultrafine PM could be attributed to the traffic conditions of the city road (i.e., stop-and-go conditions). In such traffic conditions, braking maneuvers are frequent and thus, contribute to the generation of high number of brake-wear particles [67]. The low-speed limit, i.e., 50 $km.h^{-1}$, also leads to a slow stress for the brake and as a consequence, generates brake particles with smaller diameter compared to those issued from braking at high speed. The influence of the weather on the total PM loading mass is presented in Fig. 3F for different duration and as a function of the time period between March to July 2022. According to the results, the replacement of the filter every two weeks (light blue dot) leads to a slightly higher cumulative total PM loading mass compared to the single filter left for the same cumulative period (i.e., six- and eight weeks vs. two weeks). It is worthy to note that a discrepancy in terms of PM trapping was observed for the period from 25 May to 8 June (indicated with arrow) which could be attributed to the fact that heavy rains occurred during this period which could significantly reduce the PM concentration in outdoor air. Such results could be attributed to the surface properties of the coated oil which could undergo slowly dried off, leading to a lower total PM loading mass, compared to the fresh oil coated for the sample evaluated every two weeks.

DLS analysis on various filter samples and different exposure periods show a deficit of PM under 0.3 µm of diameter. Furthermore, PM under 0.1 µm is nearly missing in both particle number and volume reports. As ultrafine particles typically originate from incomplete combustion of biomass such as wood heating and traffic emissions, the existence of PM1 is confirmed, especially in near-source environments such as residence areas or dense traffic roads [68,69]. By the reason of the limit of detection, PM concentration data includes undersize PMs in PM1. A few PM under 0.3 µm can be detected with SEM images (Fig. 7G and 7H), but their number and volume did not match the bigger range of the granulometric DLS test. Combining with the low-pressure drop of the filter structure, ultrafine particles PM0.3 are likely to follow the airflow and are less captured by the filter than by upper sizes. These results showed real potential of PM trapping from 1 to 10 µm. Particles and aerosols bigger than 10 µm like vegetable debris, dust, insects, etc. can also be trapped by clogging, and removed during the washing step. In order to assess the DLS results obtained on the passive trap we have also compared these results with those obtained in another PM monitoring site (Danube station) of the ATMO Grand Est service, equipped with a TEOM (tapered element oscillating microbalances) system, localized at few meters above the ground in the court of the front building (Solange Fernex elementary school) at a distance of ca. 30 m from our passive trapping device. The data at the same period of measurement as our passive traps were collected from the on-line website of the ATMO Grand Est (https://www.atmo-grandest.eu/). The data from the Danube station are summarized in Fig. 3E and compared with those obtained on our passive traps (Fig. 3D) for the same period of exposure. According to the results the PM distribution as a function of the ultrafine PM particle size (<1 µm) remains very

close between the two samples. The main discrepancy comes from the large PM particle size (2.5-10 μm) where a higher PM percentage was observed by the TEOM analyzer compared to the passive trapping value. Such difference could be explained by the fact that our passive trapping device is located on the ground between two traffic routes while the TEOM is located few meters above the ground. On the ground level, the passive trapping device is surrounded by vegetation which could adsorb PM_{10} with high inertital energy from the road side through inertial impaction and thus, artificially decreases its concentration while on theother side of the building, part of the PM_{10} can be lifted off by wind and being detected by the TEOM analyzer. Indeed, for small particulates, in the range of 0.05-0.5 μm, which are much small to have enough momentum for inertial impaction and thus, their capture becomes most challenging compared to large ones [70]. All in all, such comparative data confirms in part the relatively high effectiveness of the passive oil-coated traps to adsorb PMs in outdoor air.

Trapping process in outdoor environment could be significantly influenced by the PMs concentration which was directly influenced by the outdoor weather and period of time. For such assessment, two series of trap were evaluated at two different periods of the year, i.e., March and July, where the weather and the traffic induced a significant change of the PMs concentration in the outdoor air. According to the results obtained, the total PM loading mass was almost two times higher, i.e., 30 $g.m^{-2}$ (samples analyzed between June 22nd to July 20th) vs. 17 $g.m^{-2}$ (samples analyzed between March 2nd and March 30th), for the filter exposed during July (Fig. 3F). It is expected that, during July, the decrease in wind speed and the higher traffic of heavy-duty trucks could contribute to the higher PM concentration in the atmosphere which could contribute to a higher total PM loading mass [71]. The increase of the RH could also directly impact the aerodynamic size of the PMs due to secondary reactions with water droplets containing dissolved salt such as ammonium. These results indicate that such passive trapping system can offer a viable alternative for the reduction of outdoor PMs air pollution, and especially during the period of pollution peaking due to an increase of traffic.

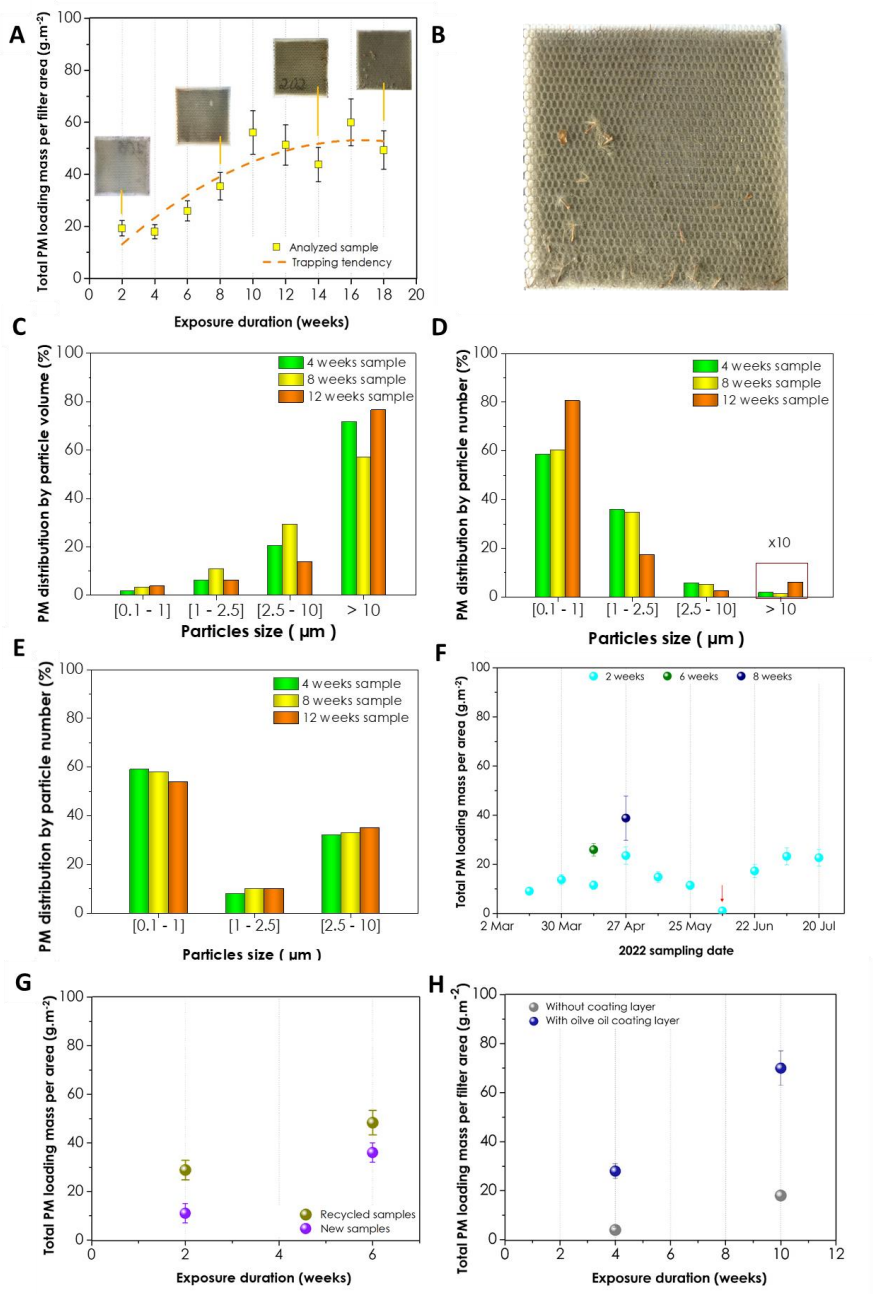

Fig. 3 | PM total PM loading mass per area as a function of time of exposure. (**A**) The average PM in weight trapped per surface unity of the filter as a function of time of exposure next to an urban area. Inset (**B**): Digital photos of the filter color as a function of time of exposure (2,8, 12 and 18 weeks). (**C**, **D**) Average distribution of the trapped PM, expressed in terms of particle size distribution in volume and in number, measured by DLS technique in the suspension after a washing step in soap-water solution at 80 °C of the spent filter after 8 weeks of time of exposure. (**E**) PM distribution by particle number, based on PM concentration data collected from ATMO Grand Est. (**F**) Weather impact monitoring using fresh samples at fixed position on the prototype (**G**) PM total loading mass per area between the fresh and regenerated filter showing the complete retention capacity of the total PM loading mass during the same period which confirms the possible re-use of the filter for several trapping processes. (**H**) PM total loading mass per area between samples with and without the oil coating layer, exposed to the same weather condition and equivalent exposure durations.

Computational simulation. Simulations were firstly carried out to assess the aerodynamics of the trap without any other obstacle and considering a perpendicular incident wind speed of 1.5 m. s^{-1} at 10 m high. According to the simulation results illustrated in Fig. 4, the airflow decreases in front of the filtration device due to the formation of vertical and horizontal vortices at the basis of the device (concrete base), but, thanks to the large porosity of the filter media, the flow increases again through the filtration device. Such numerical results confirm the relatively high flow rate passing through the filter to ensure the high PMs trapping, as the loading mass depends on the number of PMs coming in contact with the filter surface. Figure 4 presents the numerical results on airflow, specifically wind velocities and directions, obtained through computational fluid dynamics (CFD) simulations. These simulations were conducted in the absence of any obstacles and assumed a perpendicular wind direction. The primary objective was to understand how wind flows through the filter and to identify any preferential areas of flow using this filter configuration. Reproducing these conditions in a laboratory setting posed significant challenges, primarily due to the size of the device, which would have required a very large wind tunnel as those used in the aeronautic industry. Consequently, numerical modeling was employed as a viable alternative to experimentally investigate the airflow dynamics.

By using the pressure drop data from the experiments, the simulations aimed to provide a realistic representation of the airflow through the filters, ensuring the results were comparable to experimental conditions even though direct experimental replication was not feasible.

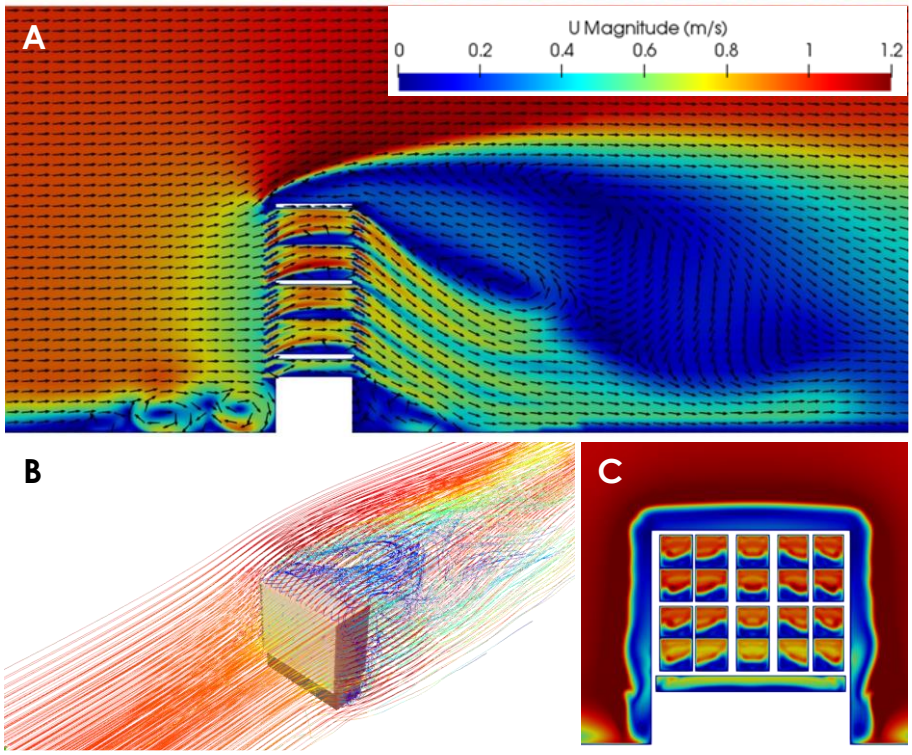

Fig. 4 | Computational fluid dynamics simulation results confirm the relatively high airflow passing per unit of time through the filter to ensure the high PMs trapping. The simulation results were based on the data, airflow and direction, furnished by the meteorology center for the area of implementation. (A) Lateral view, airflow directions are illustrated by black arrows. (B) Top view, turbulence is created on the downstream of the prototype. (C) Wind gradient shows the wind velocity distribution between cases.

The morphology of the PMs trapped on the filter as a function of time of exposure was also analyzed by SEM and the results are presented in Fig. 5. At short exposure time (2 weeks) the surface of the spent filter remains relatively well preserved due to the low density of the trapped PMs (Fig. 5A and B) despite a relatively large number of small PMs, i.e., PM_{10} and $PM_{2.5}$, can be clearly observed (Fig. 5C and D). One can also observe the presence of ultrafine PM_1 in some area of the trap (Fig. 5C). Increasing the time of exposure from 2 to 8 weeks leads to a rapid coverage of the filter surface by a large number of PM with small size as evidenced in Fig. 5E and F. Some aggregates with bigger size can also be observed on the sample after long-term exposure. Such aggregates could be generated through merging of small PM as a function of trapping time into secondary particles with bigger size (Fig. 5E), while small PMs are still being observed on the different parts of the sample (Fig. 5F). Another fact that needs to be taken into account about the size of the trapped particles is the motion and contact of the primary particle with other materials during the lap of time between their emission and their trapping. Indeed, once emitted and deposited on the road surface, tire abrasion particles could attract dust or other elements due to their intrinsic properties, i.e., flexibility and good surface adhesion, and also to their roughness. The aggregates formed thus contain not only the original primary particle but also secondary elements which are present on the shell of the particle.

Continuous exposure time up to 12 weeks leads to a high coverage of the filter surface by PMs as evidenced in Fig. 5G and H. The large aggregates become more present on the filter surface with time of exposure and are in good agreement with the hypothesis advanced above about the merging of small PM with time. However, according to the results presented in Fig. 3A the filter displays total PM loading mass up to 14 weeks despite that the slope of the curve is flattened between the twelve and fourteenth weeks.

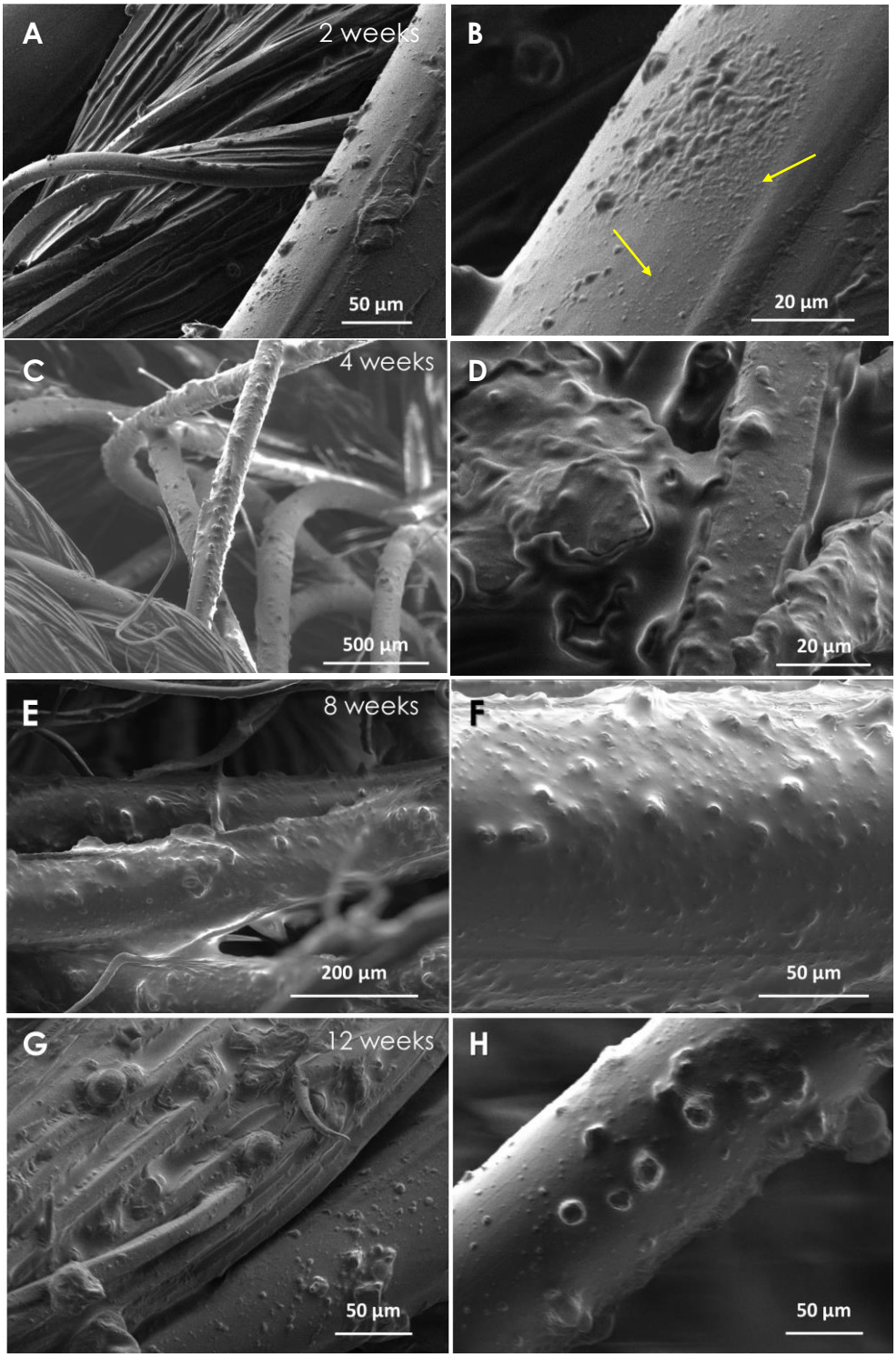

Fig. 5 | Representative SEM micrographs of the trapped PM on the structured filter as a function of time of exposure. (**A**-**B**) 2 weeks, (**C** to **D**) 4 weeks, (**E** to **F**) 8 weeks, and (**G** to **H**) 12 weeks. The as-received filters were dried at 60 °C in an oven for overnight in order to reduce the oil thickness on the top surface of the samples before the SEM analysis. The trapped PM started to aggregate from each other as a function of time of exposure leading to the formation of medium to large patches on the surface of the filter.

The representative SEM micrographs of the Aerosleep filter coated with a thin layer of olive oil are presented in Fig. 6 for comparison. On the freshly oil-coated filter, the surface is extremely smooth, and no trace of any solid particles is observed except some very tiny dots which could be due to the air exposure of the sample during the transport to the SEM apparatus.

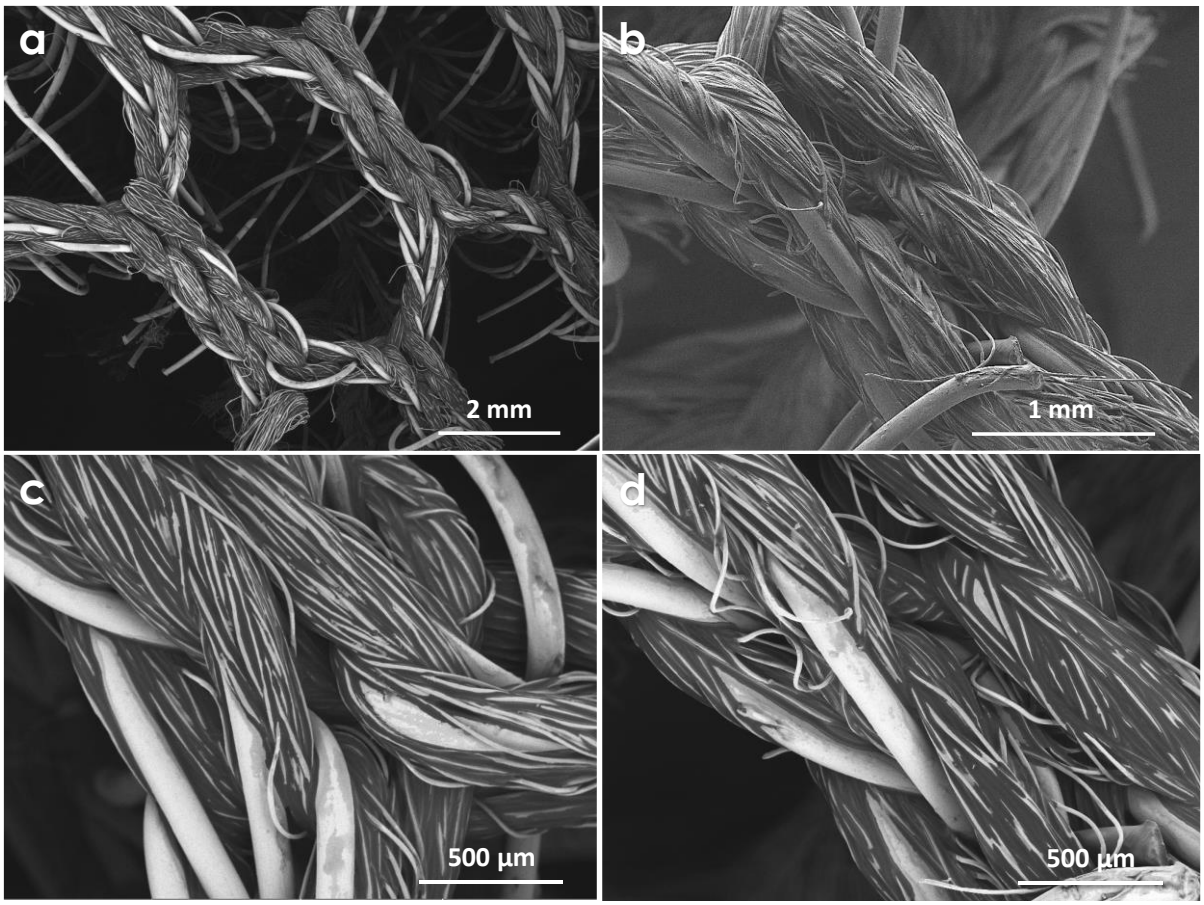

Fig. 6 | Representative SEM micrographs of the Aerosleep filter coated with a thin layer of olive oil before exposure to outdoor air displaying a clean surface.

The EDS analysis of the PM recovered on the filter after 4 weeks of exposure confirm the presence of carbon as the main constituent with some traces of metal (oxides) (Fig. 7A to F). It is expected that carbon-based material is originated from abrasion of the tires in contact with the road. Such carbon element is expected to be constituted by the tire treads which are constituted by styrene butadiene rubber which is mixed with natural rubber and additives [72]. The metal (oxide) particles, especially Ni and Al, could be issued from the car braking which release hot metal nanoparticles which are further oxidized in air. Silicon (probably in the form of silica or silicate) has also been detected in a non-negligible amount on the filter and could be attributed to be issued from the abrasion of tires during the contact with the road. However, such element cannot be exclusively ascribed to the tire wear as it is common in other road construction materials, i.e., road wear, concrete and soil. The distribution of the PMs size mapped by SEM was also evaluated and the results are presented in Fig. 7G and H and confirms the performance of the filter for trapping small particles in outdoor air. The results confirm the presence of several main elements (carbon, oxides) in the airborne PM. However, some very small particles, i.e., secondary deposition through contact with the primary particles as discussed above, could represent higher toxicity and cannot be accurately detected by the SEM technique [73,74]. In addition, it is

worthy to note that these abraded particles, regardless primary or secondary ones, can be re-suspended by either wind or turbulence create by the passing traffic, especially $PM_{2.5}$ and PM_1 with low sedimentation velocity which can remain for long duration in the atmosphere.

The size distribution of the PM trapped on the filter, according to the SEM analysis is presented in Fig. 7G and H, as a function of time of exposure, i.e., 4, 8 and 12 weeks. The results display lower fraction of fine and ultrafine PM particles compared to that observed by DLS analysis (analyzed with the same filter). Such difference could be simply explained by the fact that for SEM analysis only the visible PM on the surface can be accounted while thus located within the oil matrix are not accessible while for the DLS, all the trapped PM is accounted in the analysis. The SEM analysis also relies on the measurement of the visible PM and thus, some agglomerates of small individual PM could be accounted for one with larger size which could explain the discrepancy between the DLS and SEM methods on the particle size distribution.

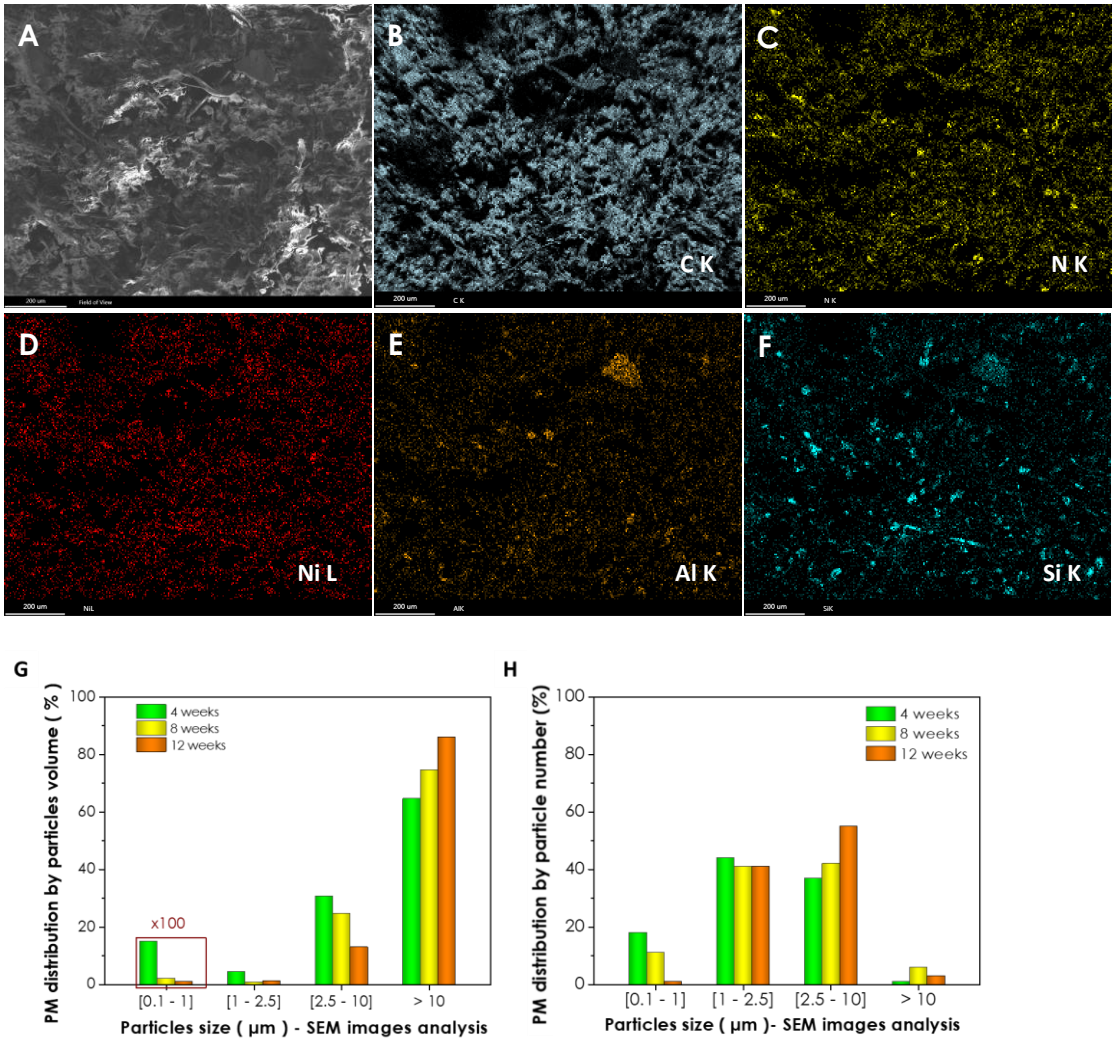

Fig. 7 | (**A**) Low magnification SEM micrograph of the trapped aggregates recovered on the filter after washing of the filter upon exposure on the test site for 4 weeks. (**B-F**) Elemental mapping of the main constituting elements in the aggregates: C, N, Ni, Al and Si. (**G**, **H**) Average particle volume and number as a function of size distribution of the recovered PM trapped determined from statistical SEM analysis. The values were determined from a counting of more than 300 particles.

TEM analysis was carried out on the suspension recovered after a water washing step of spent filters. TEM micrographs clearly evidence the presence of small particles with size ranged between 50 to 200 nm embedded in an agglomerate composite (Fig. 8A, C and E). EDS analysis indicates that these particles are mostly constituted by carbon (tire wear debris as discussed above) and oxygen but different elements such as Si (mostly as silica or silicate), Al, Fe (belonging to tires and brakes degradation) are also detected. Sulfur element was also detected in the sample and could be originated from the tires degradation, but it can also come from the asphalt as well where it could contribute to 2 to 6 wt.% depending on the origin of the bitumen [13]. Sulfur could also provide from sulfide species which are part of the lubricants. Such microscopic solid could remain long enough as airborne matter and can enter alveoli during respiration causing health problems such as cardiopulmonary disease and tracheal cancer [75,76].

Fig. 8 | Representative TEM micrographs of the trapped PM1 on the structured filter as a function of time of exposure. (**A**-**B**) 2 weeks, (**C** to **D**) 4 weeks, and (**E** to **F**) 8 weeks. The as-received filters were dried at 60 °C in an oven for overnight in order to reduce the oil thickness on the top surface of the samples before the SEM analysis. The trapped PM started to aggregate from each other as a function of time of exposure leading to the formation of medium to large patches on the surface of the filter.

Regeneration and re-use. Another parameter which could have a significant impact on the development of such a passive filter is its re-use in order to reduce its environmental impact. Indeed, the new environmental policy significantly pushes ahead the reduction of single-use devices and promotes circularity. For such evaluation the regenerated filter was coated again with an oil layer according to the recipe described in the Materials and Method section and retested for passive trapping during the same period, i.e., mid-June to mid-August with similar weather conditions and similar traffic density. The results clearly confirm the complete maintain of the total PM loading mass of the recycled filter (Fig. 3G). Such possible re-use highlights the advantage of the Aerosleep structure compared to those based on the other filters with single-use which is neither environmentally nor economically affordable despite their high filtration performance [20,21]. Representative SEM micrographs of a regenerated filter after exposure to outdoor air are presented in Fig. 9 and confirm the similar total PM loading mass as observed with a brand-new filter. Such results clearly confirm the complete regeneration and re-use of the Aerosleep filter in the present work which contribute to the reduction of the cost effectiveness of the process and its environmental impact. The possibility of re-use is also reported by Jung et al. [22] on the reduced graphene-oxide foam using model smoke at lab scale.

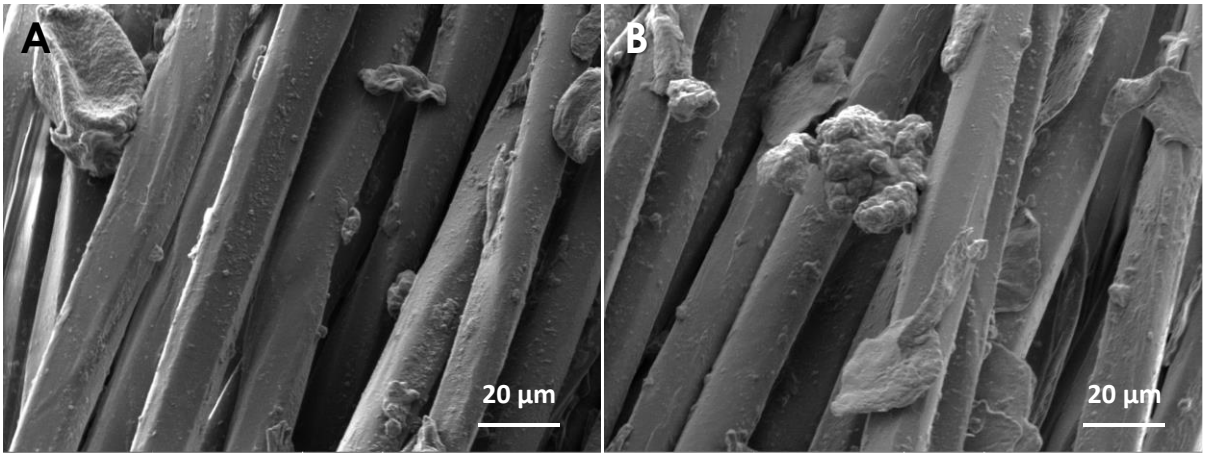

Fig. 9 | Representative SEM micrographs of the trapped PM on the re-use structured filter support, exposed 6 weeks at Rhine Avenue prototype, preceed by washing step and re-infiltration a new coating layer .

The fiber structure, capable of aerosol filtration and reusability [77], is made from a washable woven fabric of Polyethersulfone (PES) material, high liquid absorption, resistant to heat and chemical contact [78]. In function of charged PM composition and quantity, as well as the exposure duration, a filter structure can be washed and reused many times without losing its capacity of adsorption oil and PM, as long as the fibers are not damaged and lose their physical and/or chemical properties (degradation of fiber). Fig. 6A to 6D showed the effect of oil infiltration which forms a thin layer of oil on the surfaces of the fibers, and between the fibers themselves. According to researchers [46,47], this layer can play as the adsorption and retention layer of PM on the support. After the washing step, PM and most of this coating layer are removed from the fibers (see Appendix 1). This oil layer can be re-established by renewing the oil infiltration protocol with a new or regenerated support. Last but not least, this concept of regenerable air filtration support, coated by vegetable oil for outdoor passive PM trapping is promising for other materials and oil application. Regeneration would be applicable for non-damaged filter structure, as long as the structure is made from low pressure drop, washable materials, and good for oil adsorption without clogging, coupling with stable viscosity, non-toxic oil.

Simulation for upscale deployment. In this last section, a global impact on the reduction of PM_{10} for the surrounding area of the trap is investigated based on the numerical model set up with the field results obtained in previous sections. Such simulation is based on the data recovered from different organisms and will concern averaged traffic, wind direction and speed with respect to the road, and the number of filtration devices which could be safely implemented along the road for significant reduction of the emitted PMs.

As shown in Fig. 10 (A1), the study area in his actual state has high PM_{10} concentrations exceeding the annual standard value set by the EU (40 $\mu g.m^{-3}$) near the southern road lane, and, more generally in the area, exceeding WHO guidelines (15 $\mu g.m^{-3}$). Concentrations can reach 24 $\mu g.m^{-3}$ on the south side of the school building, and up to 30 $\mu g.m^{-3}$ on the sidewalk. The upscale deployment of traps can reduce these concentrations up to $\mu g.m^{-3}$ on the south side of the building school and 22 $\mu g.m^{-3}$ on the sidewalk, as depicted in Fig. 10 (A2), corresponding to an absolute PM_{10} reduction of around 3 $\mu g.m^{-3}$ and 7 $\mu g.m^{-3}$ at these locations respectively. Relatively, and without consideration of the local background concentration of 17 $\mu g.m^{-3}$, the use of the present trap induces a reduction of the PM_{10} emitted from vehicles up to 60 % next to the trap, 40 % between the trap and the school, and 10 to 15 % in the alleys adjacent to the school. Finally, as shown in Figures 10 (B1) and (B2), it should be noted that the impact of the trap on reducing ambient PM_{10} concentration is high and significant, but strongly dependent on the trap location, since its beneficial impact on the other side of the road is minimal or non-existent. Its positioning must therefore be strategic and in line with the area to be protected, while CFD modeling can help guide these choices by assessing their impact prior to trap installation.

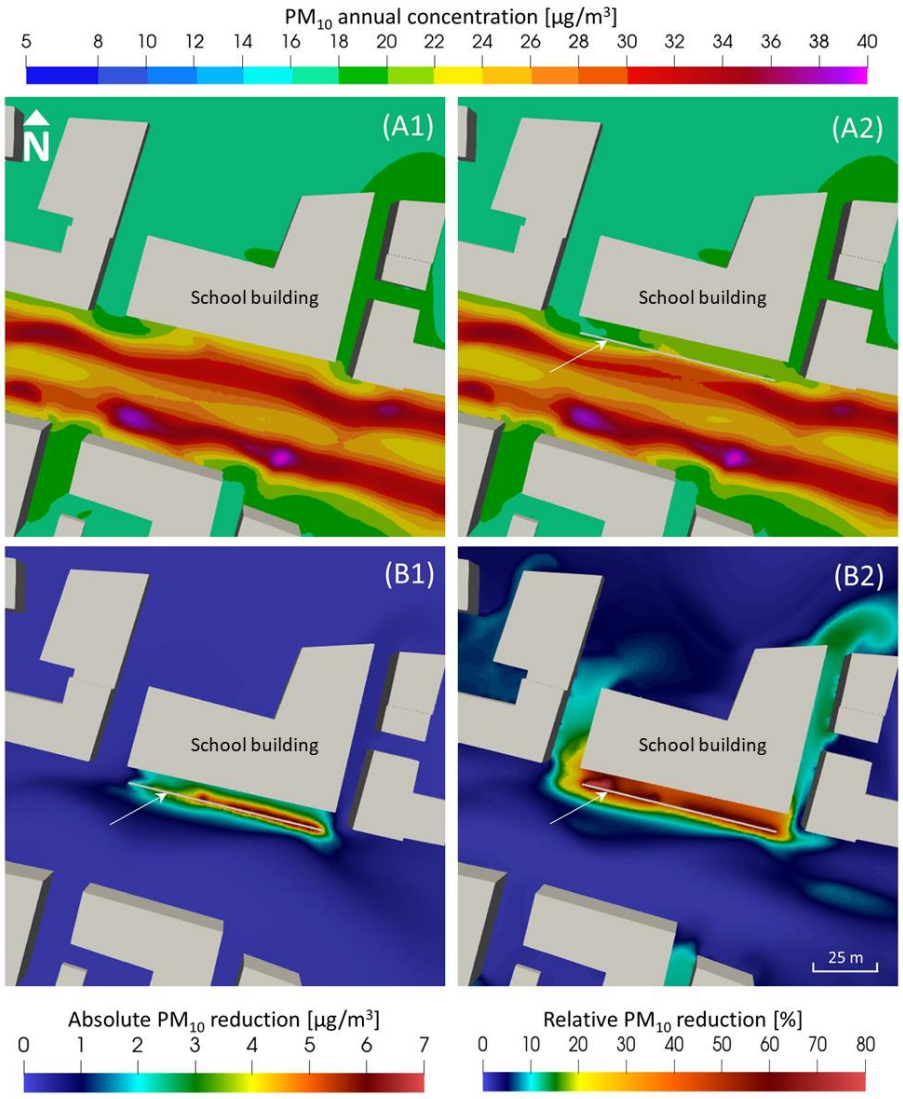

Fig. 10 | Simulation for the reduction of PM_{10} emitted from the traffic using passive trapping media in (**A1**) the actual situation without trap and (**A2**) an up-scaling deployment of the trap between the roadway and an elementary school. (**B1**, **B2**) Modeling results showing the absolute and relative total PM loading mass of the PM_{10} emitted from the traffic, respectively.

■ CONCLUSION

In conclusion, a new concept of passive coated filter for outdoor PMs trapping has been developed based on the use of a thin film of olive oil coated on a structured polyester host matrix as trapping means. The passive operating mode allows the implementation of such filter device in most of the areas where pollution needs to be reduced, such as stationary or mobile devices, without any need for connecting of the system with an external energy supply source along with a considerable reduction of the carbon footprint as usually encountered with active filtration devices. The low evaporation rate and the sticky surface of the oil film provide highly PM loading surface for airborne particulate matter as well as for long-term operation before the regeneration process, i.e. > 14 weeks. The filter developed can be operated under high natural air flux with very low-pressure drop which allows one to trap a high amount of PMs in the outdoor environment. The spent filter can be easy regenerated and reused without losing PM loading mass capacity. The loading mass remains unchanged which confirms the high stability of the system for repeated uses. The results show that PM trapped along high traffic city roads is mostly consisted with small particles which can be attributed to the low velocity of the cars and frequent stop-and-go conditions. Such passive and highly loading mass potential filter could represent an alternative for the reduction of small airborne PMs, also including $PM_{2.5}$ and more dangerously PM_1, which can seriously affect the living environments in terms of air quality and are expected to be at the origin of the reduction of life expectancy. The loading mass of the filters in the outdoor environment being, nonetheless, strongly dependent on their location, upstream studies must be conducted before placing them in order to select their best location with, for example, the help of numerical modeling such as computational fluid dynamics (CFD).

Work is ongoing to evaluate such passive traps in a semi-hermetical environment such as underground train station where large PM concentration, issued from the train braking, especially PM_1 which are unregulated nowadays, is presented which poses serious health problems for the passengers and workers.

Acknowledgements

The present work is partly financed by the AQA3P project from ADEME. The SEM experiments were carried out at the facilities of the ICPEES-IPCMS platform. The technical staffs of the Eurométropole of Strasbourg, and especially Mrs. C. Trautmann (former Vice President of the Eurométropole), are gratefully acknowledged for helpful discussion during the project. This work is also dedicated to the memory of late Mr. J.-P. Masquida.

Appendices

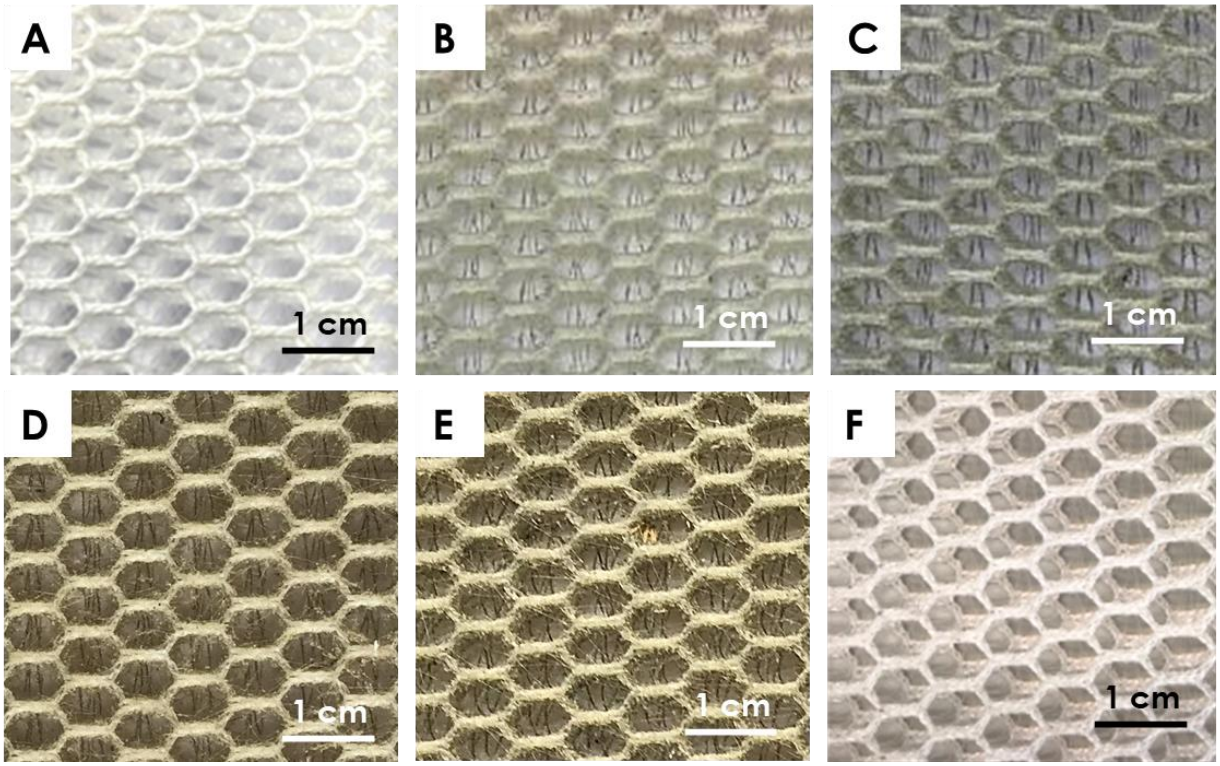

Appendix 1. Digital photos of the filter structure after exposed at outdoor Rhine Avenue prototype. **A**. 0 week; **B**. 4 weeks; **C**. 8 weeks; **D**. 12 weeks; **E**. 16 weeks; **F**. Washed and dried filter structure.

References

[1] R. Chen, B. Hu, Y. Liu, J. Xu, G. Yang, D. Xu, C. Chen, Biochim. Biophys. Acta BBA - Gen. Subj. 1860 (2016) 2844–2855.

[2] W. Chen, N. Zhang, J. Wei, H.-L. Yen, Y. Li, (2020).

[3] M.E. Deary, S.D. Griffiths, J. Hazard. Mater. 418 (2021) 126334.

[4] P. Kumar, L. Morawska, W. Birmili, P. Paasonen, M. Hu, M. Kulmala, R.M. Harrison, L. Norford, R. Britter, Environ. Int. 66 (2014) 1–10.

[5] L.-Z. Lin, X.-L. Zhan, C.-Y. Jin, J.-H. Liang, J. Jing, G.-H. Dong, Environ. Res. 209 (2022) 112876.

[6] L.N. Posner, S.N. Pandis, Atmos. Environ. 111 (2015) 103–112.

[7] D.E. Schraufnagel, J.R. Balmes, C.T. Cowl, S. De Matteis, S.-H. Jung, K. Mortimer, R. Perez-Padilla, M.B. Rice, H. Riojas-Rodriguez, A. Sood, G.D. Thurston, T. To, A. Vanker, D.J. Wuebbles, Chest 155 (2019) 417–426.

[8] H. Wang, H. Zhang, J. Li, J. Liao, J. Liu, C. Hu, X. Sun, T. Zheng, W. Xia, S. Xu, S. Wang, Y. Li, Environ. Res. 210 (2022) 112946.

[9] M. Gualtieri, J. Øvrevik, J.A. Holme, M.G. Perrone, E. Bolzacchini, P.E. Schwarze, M. Camatini, Toxicol. In Vitro 24 (2010) 29–39.

[10] C.A. Pope, Inhal. Toxicol. 19 (2007) 33–38.

[11] WHO, WHO Global Air Quality Guidelines: Particulate Matter (PM2.5 and PM10), Ozone, Nitrogen Dioxide, Sulfur Dioxide and Carbon Monoxide, WHO European Centre for Environment and Health, Bonn, Germany, 2021.

[12] H. Chen, J.C. Kwong, R. Copes, K. Tu, P.J. Villeneuve, A. Van Donkelaar, P. Hystad, R.V. Martin, B.J. Murray, B. Jessiman, A.S. Wilton, A. Kopp, R.T. Burnett, The Lancet 389 (2017) 718–726.

[13] M.M. Finkelstein, M. Jerrett, M.R. Sears, Am. J. Epidemiol. 160 (2004) 173–177.

[14] A. Peters, S. Von Klot, M. Heier, I. Trentinaglia, A. Hörmann, H.E. Wichmann, H. Löwel, N. Engl. J. Med. 351 (2004) 1721–1730.

[15] H. Zhang, S. Mao, X. Wang, Int. J. Environ. Res. Public. Health 18 (2021) 10210.

[16] N. Künzli, R. Kaiser, S. Medina, M. Studnicka, O. Chanel, P. Filliger, M. Herry, F. Horak, V. Puybonnieux-Texier, P. Quénel, J. Schneider, R. Seethaler, J.-C. Vergnaud, H. Sommer, The Lancet 356 (2000) 795–801.

[17] F. Sommer, V. Dietze, A. Baum, J. Sauer, S. Gilge, C. Maschowski, R. Gieré, Aerosol Air Qual. Res. 18 (2018) 2014–2028.

[18] M. Kooi, J. Reisser, B. Slat, F.F. Ferrari, M.S. Schmid, S. Cunsolo, R. Brambini, K. Noble, L.-A. Sirks, T.E.W. Linders, R.I. Schoeneich-Argent, A.A. Koelmans, Sci. Rep. 6 (2016) 33882.

[19] A.A. De Souza Machado, W. Kloas, C. Zarfl, S. Hempel, M.C. Rillig, Glob. Change Biol. 24 (2018) 1405–1416.

[20] R. Zhang, C. Liu, P.-C. Hsu, C. Zhang, N. Liu, J. Zhang, H.R. Lee, Y. Lu, Y. Qiu, S. Chu, Y. Cui, Nano Lett. 16 (2016) 3642–3649.

[21] C. Liu, P.-C. Hsu, H.-W. Lee, M. Ye, G. Zheng, N. Liu, W. Li, Y. Cui, Nat. Commun. 6 (2015) 6205.

[22] W. Jung, J.S. Lee, S. Han, S.H. Ko, T. Kim, Y.H. Kim, J. Mater. Chem. A 6 (2018) 16975–16982.

[23] Z. Wang, C. Zhao, Z. Pan, J. Colloid Interface Sci. 441 (2015) 121–129.

[24] J. Xiao, J. Liang, C. Zhang, Y. Tao, G.-W. Ling, Q.-H. Yang, Small Methods 2 (2018) 1800012.

[25] X. Zhang, W. Zhang, M. Yi, Y. Wang, P. Wang, J. Xu, F. Niu, F. Lin, Sci. Rep. 8 (2018) 4757.

[26] F. Schwotzer, J. Horak, I. Senkovska, E. Schade, T.E. Gorelik, P. Wollmann, M.L. Anh, M. Ruck, U. Kaiser, I.M. Weidinger, S. Kaskel, Angew. Chem. Int. Ed. 61 (2022) e202117730.

[27] H. Liu, C. Cao, J. Huang, Z. Chen, G. Chen, Y. Lai, Nanoscale 12 (2020) 437–453.

[28] D. Tan, X. Zhou, Y. Xu, C. Wu, Y. Li, Renew. Sustain. Energy Rev. 77 (2017) 1300–1308.

[29] C. Yang, Chin. J. Chem. Eng. 20 (2012) 1–9.

[30] Y. Bai, C.B. Han, C. He, G.Q. Gu, J.H. Nie, J.J. Shao, T.X. Xiao, C.R. Deng, Z.L. Wang, Adv. Funct. Mater. 28 (2018) 1706680.

[31] Y. Gao, E. Tian, J. Mo, J. Hazard. Mater. 441 (2023) 129821.

[32] S. Bourrous, L. Bouilloux, F.-X. Ouf, P. Lemaitre, P. Nerisson, D. Thomas, J.C. Appert-Collin, Powder Technol. 289 (2016) 109–117.

[33] R. Thakur, D. Das, A. Das, Sep. Purif. Rev. 42 (2013) 87–129.

[34] J. Xu, C. Liu, P.-C. Hsu, K. Liu, R. Zhang, Y. Liu, Y. Cui, Nano Lett. 16 (2016) 1270–1275.

[35] Y. Zhang, S. Yuan, X. Feng, H. Li, J. Zhou, B. Wang, J. Am. Chem. Soc. 138 (2016) 5785–5788.

[36] T. Lu, J. Cui, Q. Qu, Y. Wang, J. Zhang, R. Xiong, W. Ma, C. Huang, ACS Appl. Mater. Interfaces 13 (2021) 23293–23313.

[37] F. Amato, X. Querol, C. Johansson, C. Nagl, A. Alastuey, Sci. Total Environ. 408 (2010) 3070–3084.

[38] D. Han, H. Shen, W. Duan, L. Chen, Urban For. Urban Green. 48 (2020) 126565.

[39] J.F. Gomes, J. Bordado, A. Paula, J. Toxicol. Environ. Health A 85 (2012) ii–ii.

[40] J. Gomes, P. Albuquerque, H.M.D.S. Esteves, P.A. Carvalho, Energy Emiss. Control Technol. (2013) 15.

[41] X. Jurado, N. Reiminger, L. Maurer, J. Vazquez, C. Wemmert, Atmosphere 14 (2023) 385.

[42] X. Jurado, N. Reiminger, M. Benmoussa, J. Vazquez, C. Wemmert, Expert Syst. Appl. 203 (2022) 117294.

[43] X. Jurado, N. Reiminger, L. Maurer, J. Vazquez, C. Wemmert, Sustain. Cities Soc. 99 (2023) 104951.

[44] J.-P. Masquida, C. Pham, H. Ba, M. Millet, J.-M. Jeltsch, J.-A. Héraud, J. Laurent, C. Pham-Huu, Eléments de Construction Pour l'assainissement Du Milieu Urbain Routier, n.d.

[45] C. Pham, C. Vieville, N. Hertel, J.-M. Nhut, H. Ba, F. Vigneron, L. Truong-Phuoc, C. Pham-Huu, Dispositif Passif de Capture Des Microparticules En Suspension Dans l'air, n.d.

[46] I.E. Agranovski, in: I. Agranovski (Ed.), Aerosols - Sci. Technol., Wiley-VCH Verlag GmbH & Co. KGaA, Weinheim, Germany, 2010, pp. 315–342.

[47] T.K. Müller, J. Meyer, E. Thébault, G. Kasper, Powder Technol. 253 (2014) 247–255.

[48] V. Yakhot, S.A. Orszag, S. Thangam, T.B. Gatski, C.G. Speziale, Phys. Fluids Fluid Dyn. 4 (1992) 1510–1520.

[49] J. Franke, A. Baklanov, Best Practice Guideline for the CFD Simulation of Flows in the Urban Environment: COST Action 732 Quality Assurance and Improvement of Microscale Meteorological Models, 2007.

[50] N. Reiminger, X. Jurado, J. Vazquez, C. Wemmert, N. Blond, M. Dufresne, J. Wertel, J. Wind Eng. Ind. Aerodyn. 200 (2020) 104160.

[51] P.J. Richards, S.E. Norris, J. Wind Eng. Ind. Aerodyn. 99 (2011) 257–266.

[52] N. Reiminger, J. Vazquez, N. Blond, M. Dufresne, J. Wertel, J. Wind Eng. Ind. Aerodyn. 196 (2020) 104032.

[53] E. Rivas, J.L. Santiago, Y. Lechón, F. Martín, A. Ariño, J.J. Pons, J.M. Santamaría, Sci. Total Environ. 649 (2019) 1362–1380.

[54] M. Ekström, Å. Sjödin, K. Andreasson, Atmos. Environ. 38 (2004) 6631–6641.

[55] N. Reiminger, X. Jurado, J. Vazquez, C. Wemmert, N. Blond, J. Wertel, M. Dufresne, Sustain. Cities Soc. 59 (2020) 102221.

[56] X. Jurado, N. Reiminger, J. Vazquez, C. Wemmert, Sustain. Cities Soc. 71 (2021) 102920.

[57] M. Lacroix, P. Nguyen, D. Schweich, C. Pham Huu, S. Savin-Poncet, D. Edouard, Chem. Eng. Sci. 62 (2007) 3259–3267.

[58] Q. Royer, R. Guibert, P. Horgue, A. Swadling, G. Debenest, Int. J. Heat Mass Transf. 226 (2024) 125438.

[59] K. Okamoto, N. Watanabe, Y. Hagimoto, K. Miwa, H. Ohtani, Fire Saf. J. 44 (2009) 756–763.

[60] L. So Khuong, N. Hashimoto, Y. Konno, Y. Suganuma, H. Nomura, O. Fujita, Fuel 368 (2024) 131604.

[61] M.C. Ramírez-Tortosa, S. Granados, J.L. Quiles, in: J.L. Quiles, M.C. Ramírez-Tortosa, P. Yaqoob (Eds.), Olive Oil Health, 1st ed., CABI, UK, 2006, pp. 45–62.

[62] D. Boskou, Olive Oil, 0 ed., AOCS Publishing, 2006.

[63] A.H. Rantamäki, M. Javanainen, I. Vattulainen, J.M. Holopainen, Investig. Opthalmology Vis. Sci. 53 (2012) 6442.

[64] M. Tang, S.-C. Chen, D.-Q. Chang, X. Xie, J. Sun, D.Y.H. Pui, Sep. Purif. Technol. 198 (2018) 137–145.

[65] E. Iritani, N. Katagiri, G. Inagaki, Sep. Purif. Technol. 198 (2018) 3–9.

[66] A. Peters, H.E. Wichmann, T. Tuch, J. Heinrich, J. Heyder, Am. J. Respir. Crit. Care Med. 155 (1997) 1376–1383.

[67] T. Grigoratos, G. Martini, Environ. Sci. Pollut. Res. 22 (2015) 2491–2504.

[68] C.-C. Lin, S.-J. Chen, K.-L. Huang, W.-I. Hwang, G.-P. Chang-Chien, W.-Y. Lin, Environ. Sci. Technol. 39 (2005) 8113–8122.

[69] Y. Zhu, W.C. Hinds, S. Kim, C. Sioutas, J. Air Waste Manag. Assoc. 52 (2002) 1032–1042.

[70] C.-S. Wang, Powder Technol. 118 (2001) 166–170.

[71] T. Le, Y. Wang, L. Liu, J. Yang, Y.L. Yung, G. Li, J.H. Seinfeld, Science 369 (2020) 702–706.

[72] Sundt P., Syversen F., Skogesal O., Schulze P. E, (2015).

[73] K. Malachova, J. Kukutschova, Z. Rybkova, H. Sezimova, D. Placha, K. Cabanova, P. Filip, Ecotoxicol. Environ. Saf. 131 (2016) 37–44.

[74] A. Wik, G. Dave, Chemosphere 64 (2006) 1777–1784.

[75] R.M. Harrison, J. Yin, Sci. Total Environ. 249 (2000) 85–101.

[76] S. Jeong, H. Cho, S. Han, P. Won, H. Lee, S. Hong, J. Yeo, J. Kwon, S.H. Ko, Nano Lett. 17 (2017) 4339–4346.

[77] J. Howarth, S. Anand, Text. Res. J. 86 (2016) 1962–1972.

[78] L.W. McKeen, in: Fluorinated Coat. Finish. Handb., Elsevier, 2006, pp. 45–58.